Mechanistic analysis of allosteric and non-allosteric effects arising from nanobody binding to two epitopes of the dihydrofolate reductase of Escherichia coli

ARTICLE *in* BIOCHIMICA ET BIOPHYSICA ACTA · JULY 2013

Impact Factor: 4.66 · DOI: 10.1016/j.bbapap.2013.07.010 · Source: PubMed

5 AUTHORS, INCLUDING:

David Oyen
The Scripps Research Institute
5 PUBLICATIONS **17** CITATIONS
SEE PROFILE

Vasundara Srinivasan
Philipps University of Marburg
20 PUBLICATIONS **277** CITATIONS
SEE PROFILE

Jan Steyaert
Vrije Universiteit Brussel
136 PUBLICATIONS **4,715** CITATIONS
SEE PROFILE

John N Barlow
GlaxoSmithKline plc.
15 PUBLICATIONS **321** CITATIONS
SEE PROFILE

Biochimica et Biophysica Acta 1834 (2013) 2147–2157

Contents lists available at ScienceDirect

Biochimica et Biophysica Acta

journal homepage: www.elsevier.com/locate/bbapap

Mechanistic analysis of allosteric and non-allosteric effects arising from nanobody binding to two epitopes of the dihydrofolate reductase of *Escherichia coli*

David Oyen [a,b], Rainer Wechselberger [c], Vasundara Srinivasan [a,b], Jan Steyaert [a,b], John N. Barlow [a,b,*]

[a] Structural Biology Brussels, Vrije Universiteit Brussel, Pleinlaan 2, 1050 Brussels, Belgium
[b] Structural Biology Research Centre, VIB, Pleinlaan 2, 1050 Brussels, Belgium
[c] Large Scale Facility, NMR Spectroscopy, Bijvoet Centre for Biomolecular Research, Padualaan 8, NL-3584 CH Utrecht, The Netherlands

ARTICLE INFO

Article history:
Received 21 May 2013
Received in revised form 22 July 2013
Accepted 24 July 2013
Available online 31 July 2013

Keywords:
Enzyme
Antibody
Allostery
NMR
Crystallography

ABSTRACT

Although allosteric effector antibodies are used widely as modulators of receptors and enzymes, experimental analysis of their mechanism remains highly challenging. Here, we investigate the molecular mechanisms of allosteric and non-allosteric effector antibodies in an experimentally tractable system, consisting of single-domain antibodies (nanobodies) that target the model enzyme dihydrofolate reductase (DHFR) from *Escherichia coli*. A panel of thirty-five nanobodies was isolated using several strategies to increase nanobody diversity. The nanobodies exhibit a variety of effector properties, including partial inhibition, strong inhibition and stimulation of DHFR activity. Despite these diverse effector properties, chemical shift perturbation NMR epitope mapping identified only two epitope regions: epitope α is a new allosteric site that is over 10 Å from the active site, while epitope β is located in the region of the Met20 loop. The structural basis for DHFR allosteric inhibition or activation upon nanobody binding to the α epitope was examined by solving the crystal structures of DHFR in complex with Nb113 (an allosteric inhibitor) and Nb179 (an allosteric activator). The structures suggest roles for conformational constraint and altered protein dynamics, but not epitope distortion, in the observed allosteric effects. The crystal structure of a β epitope region binder (ca1698) in complex with DHFR is also reported. Although CDR3 of ca1698 occupies the substrate binding site, ca1698 displays linear mixed inhibition kinetics instead of simple competitive inhibition kinetics. Two mechanisms are proposed to account for this apparent anomaly. Evidence for structural convergence of ca1698 and Nb216 during affinity maturation is also presented.

1. Introduction

A variety mechanisms have evolved that allow enzyme and receptor activity to be controlled by other proteins *in vivo*. One important regulation mechanism involves the binding of an inhibitory protein into the active site region, as exemplified by many proteases [1], amylases [2] and RNases [3]. Alternatively, enzyme and receptor function can be modulated by proteins, termed allosteric effectors, that bind to regions outside of the active site [4,5]. The best characterised allosteric effector proteins are antibodies and their fragments. Antibody binding to enzymes can give rise to a variety of kinetic effects that are consistent with antibody binding to epitopes distal to the active site, such as stimulation of enzyme activity [6–8] and non-competitive inhibition [9,10]. In the majority of cases, the molecular basis for these allosteric effects remains poorly understood, in part, because of the large sizes of antibody/enzyme and antibody/receptor complexes. A better understanding could facilitate the development of new therapeutic antibodies[11] and new antibody-based tools for studying allosteric systems [12].

We have developed a model experimental system to study the mechanisms of antibody allosteric effectors that consists of the enzyme dihydrofolate reductase from *E. coli* (DHFR) modulated by single domain antibody fragments (nanobodies) [13]. This system is amenable to analysis using a wide variety of experimental techniques (such as stopped-flow and NMR spectroscopy) that permit allosteric effects to be dissected at the molecular level. Both conformational change and protein dynamics play prominent roles in DHFR catalysis [14,15]. DHFR contains two subdomains termed the adenosine binding subdomain (residues 38–88) and the loop subdomain. Crystallographic studies have identified the structures of all the intermediates on the catalytic cycle [16]. Notably, they show that the loop subdomain contains a flexible active site loop, termed the Met20 loop, that cycles between two different conformations during catalysis (termed the occluded and closed states). The protein dynamics of these intermediates, or structural analogues of these intermediates, have been investigated using

Abbreviations: DHFR, dihydrofolate reductase; Nb, nanobody; NMR, nuclear magnetic resonance; DHF, dihydrofolate; NADPH, reduced nicotinamide adenine dinucleotide phosphate; THF, tetrahydrofolate; CDR, complementarity-determining region; PBS, phosphate-buffered saline; ELISA, enzyme-linked immuno sorbent assay; PDB, Protein Data Bank

* Corresponding author at: GSK Vaccines, Rue de l'institut 89, 1330 Rixensart, Belgium. Tel.: +32 2 6565651.
E-mail address: John.N.Barlow@GSK.COM (J.N. Barlow).

1570-9639/$ – see front matter © 2013 Elsevier B.V. All rights reserved.
http://dx.doi.org/10.1016/j.bbapap.2013.07.010

NMR spectroscopy. For example, R_2 relaxation dispersion experiments indicate that each intermediate can sample excited states whose structures resemble the structure of the preceding and/or succeeding intermediate on the catalytic pathway [17]. Therefore, this system also provides an opportunity to examine allosteric effects that result from constraint of functional conformational change and protein dynamics. The ability of nanobodies to constrain conformational change, leading to hyperbolic inhibition, was shown for the allosteric effector nanobody Nb216 [13]. By contrast, the role played by protein dynamics in allosteric effector antibody mechanisms remains unclear. Recent statistical coupling analysis and (allosteric) domain insertion scanning studies of DHFR support the existence of allosteric regulation hot spots in DHFR [18]. It has also been demonstrated that antibodies can perturb antigen protein dynamics [19]. It is therefore of great interest to determine the type and magnitude of kinetics that are induced upon binding of antibodies to such allosteric hotspots.

Here, we describe efforts to isolate a panel of allosteric effector nanobodies that target DHFR. Several allosteric effectors are identified and are shown to bind to the same epitope region, despite giving rise to contrasting allosteric effects. The structural basis for these allosteric effects is investigated using X-ray crystallography. We also show for the first time that the occupancy of an active site by a nanobody CDR loop does not necessarily lead to pure competitive inhibition. Finally, we present evidence for structural convergence during affinity maturation between two antibodies from different germline B lymphocytes.

2. Methods

2.1. General procedures

A pET22b-dervied expression vector containing the coding sequence of DHFR from Escherichia coli was kindly provided by Professor S. Benkovic (University of Pennsylvania). DHFR was purified according to the method described by Boehr et al. [17]. DHF was prepared from folic acid [20].

2.2. Immunisation and phage library generation

Two llamas were immunised with six doses of 200 mg of purified recombinant *E. coli* DHFR over a period of 6 weeks. One llama (+) was immunised with antigen mixed with Gerbu adjuvant (a colloidal suspension of cationic lipid nanoparticles containing N-acetylglucosaminyl-N-acetylmuramyl-L-alanyl-D-isoglutamine and cimetidine); the other llama (−) was immunised without adjuvant. Phage libraries were prepared from each llama using standard protocols [21].

2.3. Nanobody selection by phage Panning

Three panning methods were used to select phage particles expressing DHFR-specific nanobodies. In Method 1, DHFR was coated onto methotrexate-agarose beads. 0.3 ml beads (settled volume, Sigma) were first extensively washed in PBS to remove free methotrexate

Table 1
Summary of nanobody properties.

Nanobody	Library	k_{on}/μM^{-1} s^{-1}	k_{off}/s^{-1}	K_D/nM	Epitope	Kinetic effect[a]
120[b]	(−)	4.4	0.01	2	α	Partial inhibition
122	(−)	ND[c]	ND	>500[d]		ND
119	(−)	ND	ND	>500		ND
113	(−)	3	0.009	3	α	Partial inhibition
179[b]	(−)	0.71	0.016	23	α	Activation
121[b]	(−)	1.5	0.0015	1		Inhibition
114	(−)	0.91	0.073	80		No effect
117[b]	(−)	1.6	0.026	16		No effect
118b[e]	(−)	0.9	0.03	38	α	No effect
216	(+)	0.078	0.004	54	β	Strong inhibition
217	(+)	0.34	0.026	77		No effect
214	(+)	ND	ND	>500		Inhibition
219	(+)	0.039	0.002	51		Inhibition
215	(+)	0.030	0.001	33		Inhibition
220	(+)	ND	ND	>500		Inhibition
221	(+)	0.29	0.025	86	β	Inhibition
218	(+)	0.33	–	316[f]		No effect
223	(+)	0.09	0.03	372		Inhibition
222	(+)	0.07	0.03	388		Inhibition
CA1687	Combined	0.43	0.006	14		No effect
CA1688	Combined	0.20	0.1	555	β	Strong inhibition
CA1689	Combined	1.65	0.003	2	α	No effect
CA1690	Combined	0.10	0.003	28	β	No effect
CA1691	Combined	0.80	0.012	16		No effect
CA1692	Combined	0.35	0.002	6	α	No effect
CA1694	Combined	0.19	0.001	6	β	Strong inhibition
CA1695	Combined	ND	ND	>500		No effect
CA1696	Combined	1.11	0.002	2	α	No effect
CA1697	Combined	0.11	0.003	30	β	Strong inhibition
CA1698	Combined	0.48	–	1[f]	β	Strong inhibition
CA1699	Combined	0.15	0.001	7	β	ND
CA1700	Combined	0.09	0.0004	4	β	Strong inhibition
CA1701	Combined	1.4	0.005	3	α	No effect
CA1702	Combined	0.44	0.0006	1		Strong inhibition
CA1703	Combined	0.25	0.0002	0.9	β	Strong inhibition

[a] Observed effect during screening (10 μM DHF, 5 μM NADPH, vary [Nb] from 0 to 1 μM or 4 μM).
[b] Isolated using methotrexate-agarose beads.
[c] Not determined.
[d] Binding not observed on Biacore at the highest (0.5 μM) DHFR concentrations used.
[e] Isolated by both ELISA plate and methotrexate-agarose bead panning methods.
[f] Two-step binding model gives a better fit than a 1:1 Langmuir binding model.

(checked by measuring the spectrum of the wash). Following washing, 1 ml of 15 μM DHFR in PBS was added and left at room temperature for 15 min. A control tube containing 1 ml of PBS and 0.3 ml of bead stock was also made. The two bead samples were then washed extensively in PBS and re-suspended in blocking solution (3% BSA in PBS with rotation for 2 h at room temperature). The blocking solution was removed by washing in PBS and phage stock added (10^{11} particles per tube) and left for 1 h with rotation at room temperature. Unbound phages were then washed off with extensive washing (two washes in 1 ml PBS, followed by two washes in 40 ml PBS). Bound phage were eluted by incubation with TEA (100 μl) for 10 min at room temperature. Tests showed that essentially all of the added DHFR remains bound to the bead during extensive washing, but is eluted in the TEA buffer used for phage eluted. The beads were centrifuged and the supernatant used for phage amplification and for determination of the enrichment factor. In method 2, phage were panned against DHFR coated onto plastic ELISA plates (10 μg/well) [22]. In method 3, biotinylated DHFR was bound to neutravidin-coated ELISA plates to minimise DHFR denaturation that can potentially occur during direct absorption to the ELISA plate. DHFR (1 mL of a 0.036 mM DHFR solution in 0.1 M Phosphate, 0.15 M NaCl, pH 7.2) was biotinylated using a 20-fold molar excess of EZ-link™ Sulfo-NHS-SS-Biotin linker (73 μL of a 6 mg/mL solution; Thermo Scientific). The reaction was incubated for two hours on ice and quenched with 20 μL of a 1 M Tris solution (pH 7.5). Un-reacted linker was removed by dialysis. We determined an average of 1.4 biotin molecules per DHFR molecule (HABA biotin quantification kit, Thermo Scientific). The biotinylated DHFR displayed normal to slightly reduced activity in a steady state essay under saturated ligand concentrations. For each panning method, three rounds of panning were performed. Phage enrichment, phage binding specificity and DNA sequence diversity were assessed using standard methods [22].

2.4. Nanobody production

Nanobodies were produced in *E. coli* WK6 from the pHEN6 vector using Ni-affinity and size exclusion chromatography, as previously described [21]. Typical yields were 5–10 mg nanobody from 1 l of media. Nanobodies were stored in 50 mM phosphate, 150 mM NaCl, pH 7.0 at 4 °C or −20 °C. Some nanobody preparations contained significant quantities of contaminating DHFR (generally 1 part in 10,000) and were not suitable for steady-state kinetic analysis. We therefore used a DHFR knock-out expression host (*E. coli* LH8, kindly provided by Professor Liz Howell, University of Tennessee). The protocol for nanobody production in the LH8 strain was identical to that used for the WK6 strain, except that LH8 cultures were grown in TB broth supplemented with kanamycin, ampicillin and thymidine (50 μg/ml). The yield of nanobody obtained was generally 10–20% lower from the LH8 strain than from the WK6 strain.

2.5. Kinetic and affinity of measurements of nanobody-DHFR interactions

Association and dissociation rate constants were measured by surface plasmon resonance (Biacore T100) at 25 °C using nanobodies immobilised to a nickel-nitrilotriacetic acid biochip [8].

2.6. Steady-state assays of DHFR

Assays were performed using a standard protocol [13]. A microplate assay format (Nunc Polysorp 96-well plate) was used during the screening of the combined library nanobodies. DHFR (0.5 nM) was pre-incubated in the microplate for 10 min at 25 °C with nanobody (1 μM) and NADPH (0–40 μM) in MTEN buffer (supplemented with Triton X-100 (0.01%) to reduce the surface meniscus) in a final volume of 100 μl. The reaction was initiated by the addition of DHF (100 μl of a 20 μM) and the decrease in absorbance measured at 340 nm using a Tecan plate reader. Controls containing no nanobody were included on each microplate. For the detailed kinetic analysis of Nb113 and Nb179, plots of apparent $(K_m/k_{cat})^{NADPH}$ and apparent $(1/k_{cat})^{NADPH}$ *versus* nanobody concentration were fitted to Eq. (1) [13]:

$$y = a \times \frac{(1 + [Nb]/K_{num})}{(1 + [Nb]/K_{denom})} \quad (1)$$

ca1698 inhibition kinetics were measured at fixed NADPH (50 μM) and varying DHF. Plots of apparent $(K_m/k_{cat})^{DHF}$ and apparent $(1/k_{cat})^{DHF}$ *versus* nanobody concentration were fitted to Eqs. (2) and (3), derived from the mixed inhibition Eq. (4):

$$\left(\frac{1}{k_{cat}}\right)^{apparent} = \left(\frac{1}{k_{cat}}\right) + \left(\frac{1}{k_{cat}K_{iu}}\right) \times [CA1698] \quad (2)$$

$$\left(\frac{K_m}{k_{cat}}\right)^{apparent} = \left(\frac{K_m}{k_{cat}}\right) + \left(\frac{K_m}{k_{cat}K_{ic}}\right) \times [CA1698] \quad (3)$$

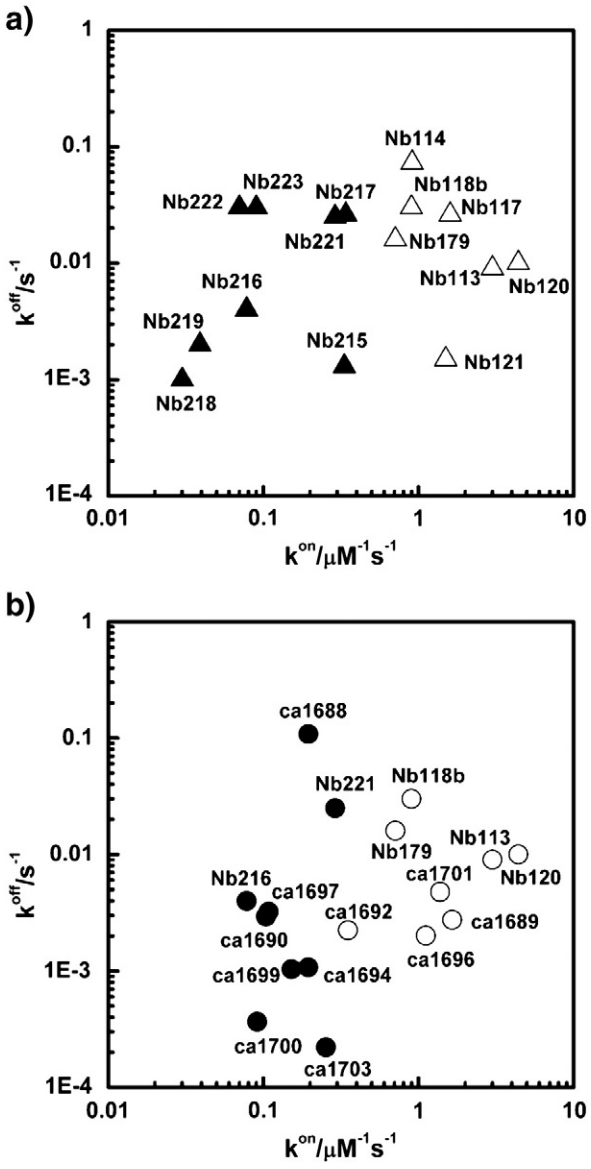

Fig. 1. Plots of k^{off} *versus* k^{on} for DHFR binding to immobilised nanobodies. (a) Nanobodies from the (+) and (−) libraries are shown as filled and open triangles, respectively. (b) Nanobodies that bind to the β and α epitope regions are shown as filled circles and open circles, respectively.

$$v = \frac{V.[DHF]}{K_m\left(1+\frac{[ca1698]}{K_{ic}}\right)+\left(1+\frac{[ca1698]}{K_{iu}}\right)[DHF]} \quad (4)$$

where K_{ic} = the competitive inhibition constant and K_{iu} = the uncompetitive inhibition constant at 50 μM NADPH.

2.7. Epitope mapping by chemical shift perturbation NMR

^{15}N-labelled DHFR was produced according the protocol of Boehr et al. [17] and stored at −80 °C in storage buffer (25 mM Tris, 1 mM EDTA, 1 mM DTT, 200 mM NaCl, 20% glycerol, pH 7.5). Immediately prior to NMR measurement, nanobody and DHFR solutions were exchanged into NMR buffer (5 mM sodium phosphate, 50 mM NaCl, 5% ^2H_2O, pH 6.8 at room temperature) using PD10 desalting columns. After measuring the UV/Vis spectra, the nanobody and DHFR samples were mixed in a 1.5:1 molar ratio (nanobody:DHFR). Filtered solutions of D12 EDTA and folate in NMR buffer were then added to a final concentration of 1 mM for each. The sample was then concentrated using a spin concentrator to a final [DHFR.folate.nanobody] ternary complex concentration of 0.5 mM and transferred to an NMR tube (Norell Select Series 5 mm, 600 MHz). ^{1}H–^{15}N–HSQC spectra were measured on a 900 MHz Bruker NMR spectrometer fitted with cryoprobe at 25 °C.

^{1}H–^{15}N HSQC spectra were analysed using the UNIX-based program Sparky (T. D. Goddard and D. G. Kneller, SPARKY 3, University of California, San Francisco). Peaks of the 15N-labelled DHFR:folate HSQC spectrum were identified using the previously reported resonance assignments of the binary folate complex of DHFR [23]. This spectrum was used as the reference spectrum during the chemical shift perturbation analysis of [DHFR.folate.nanobody] 1H–15N HSQC spectra. Cross peaks in the [DHFR.folate.nanobody] spectra were assigned to one of four categories according to the magnitude of the chemical shift perturbation [24]: i) strongly affected cross peaks (peaks perturbed more than two line widths away from the reference spectrum); ii) weakly affected cross peaks (peaks displaying a reduced intensity or shifted within two line widths of the original cross peak); iii) un-perturbed cross peaks; and iv) residues excluded from the analysis.

2.8. Crystallography

DHFR-nanobodies complexes were purified by size-exclusion chromatography (Supedex 75) and concentrated. The following crystallization conditions were used with sitting drop vapor diffusion method at 298 K: (DHFR:Nb113) 25.5% w/v PEG4000, 0.085 M NaCitrate pH 5.6, 0.17 M Ammonium Sulphate, 25% Glycerol; (DHFR:folate:NADP:Nb179) 25% w/v PEG 4000; 0.1 M Na HEPES pH 7.5; 0.2 M Sodium Chloride; (DHFR:Ca1698) 20% PEG w/v 1500, 0.1 M Tris pH 7.5, 0.1 M Ammonium Sulphate. Crystals were apparent between 1 and 2 weeks and cryopreserved directly. Datasets were collected at the SLS beam line X06DA and the ESRF beam lines BM14 and ID23-1. Data collection and processing statistics and methods are detailed in SI Table 1. Briefly, the data for the DHFR:Nb113, DHFR:Ca1698 and the DHFR:folate:NADP:Nb179 complexes were processed using Mosfilm and CCP4 suite of programs. The structure was solved using the molecular replacement method with PHASER and further refined using PHENIX refinement.

3. Results

3.1. Isolation of nanobodies from two llamas by phage display

A panel of 35 nanobodies were isolated from two llamas using phage display technology (Table 1). The llamas were immunised with DHFR in the presence (+) or absence (−) of adjuvant. In order to select (potentially rare) nanobodies that bind to epitopes distal to the active site, we panned the two phage libraries separately against DHFR bound to methotrexate-agarose beads. Methotrexate binds to the DHFR substrate binding site with high affinity, leading to masking of active site epitopes by the affinity ligand. Enrichment of DHFR-specific phage using methotrexate-agarose beads was seen with the (−) phage library but not with the (+) phage library. This indicates that only the (−) library contained nanobodies that bind to epitopes that are distal to the substrate binding site. Enrichment of phage from both libraries was seen during panning with DHFR absorbed directly on ELISA plates. This was performed in order to select allosteric effectors that bind in the vicinity of the active site. Nanobodies were also obtained by panning

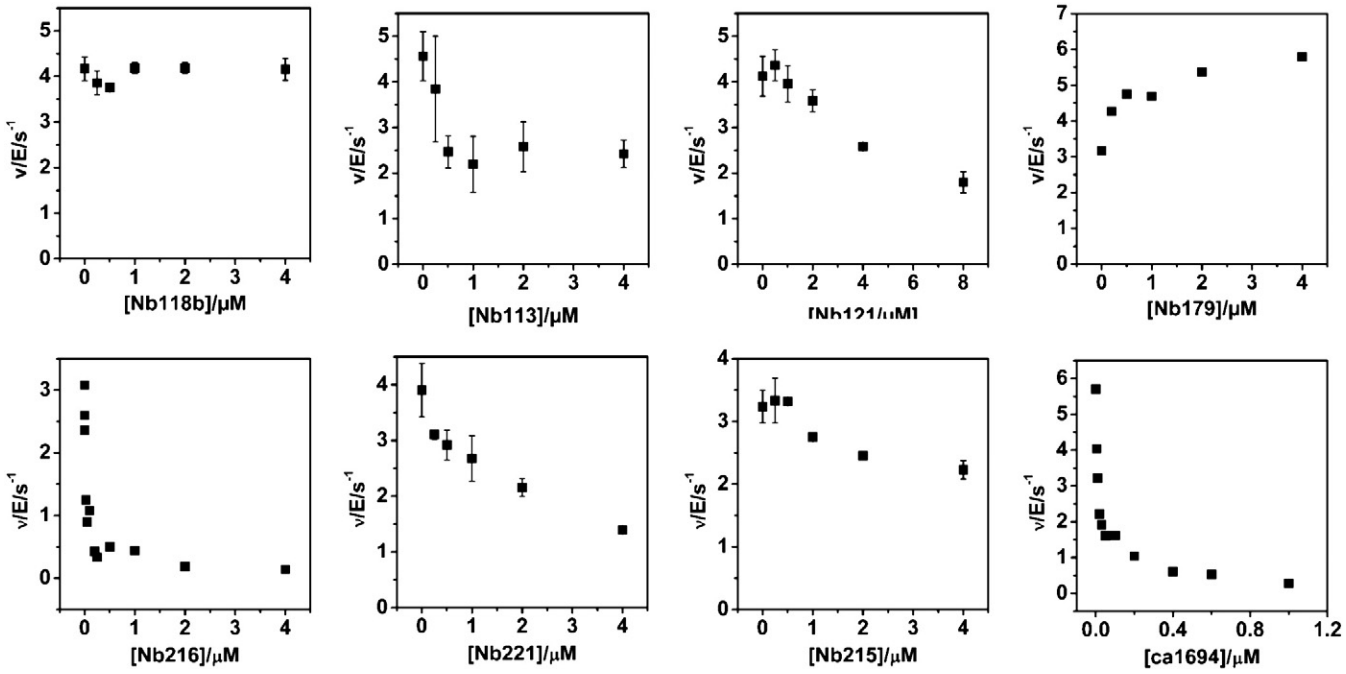

Fig. 2. A selection of nanobody kinetic profiles measured at 25 °C. Error bars (where shown) represent the standard deviation from two experiments. Note that the nanobody concentration range varies between the nanobodies.

the combined libraries against biotinylated DHFR immobilised on a streptavidin coated ELISA plate (Table 1).

3.2. Nanobodies cluster into two groups according to their association rate constants

Prior to examining the effector properties of the nanobodies, we measured DHFR-nanobody affinities in order to determine the nanobody concentrations required for steady-state kinetic analysis. The nanobody dissociation constants vary from sub-nanomolar to micromolar, as determined by surface plasmon resonance (Table 1 and SI Fig. 2). Interestingly, nanobodies isolated from the (+) library display association rate constants (k_{on}'s) that are 15-fold lower on average than those from the (−) library ($0.13 \pm 0.12\ \mu M^{-1}\ s^{-1}$ *versus* $1.9 \pm 1.4\ \mu M^{-1}\ s^{-1}$, Fig. 1a). By contrast, the dissociation rate constants do not show any clustering.

3.3. Nanobodies display diverse kinetic effects on DHFR steady-state activity

In order to identify potential allosteric effector nanobodies, we screened the nanobody panel using a DHFR steady-state kinetic assay at constant NADPH and DHF concentrations and varying nanobody concentration (Fig. 2). A variety of kinetic profiles are seen, including no effect, partial inhibition, stimulation, inhibition and strong inhibition (loss of DHFR activity when [Nb] ~ K_D). Notably, the observation of partial inhibition and stimulation of DHFR by (−) nanobodies is indicative of allosteric effector behaviour.

3.4. Two epitope regions are identified using chemical shift perturbation NMR

In order to confirm that allosteric effector nanobodies had been isolated, we performed epitope mapping using chemical shift perturbation

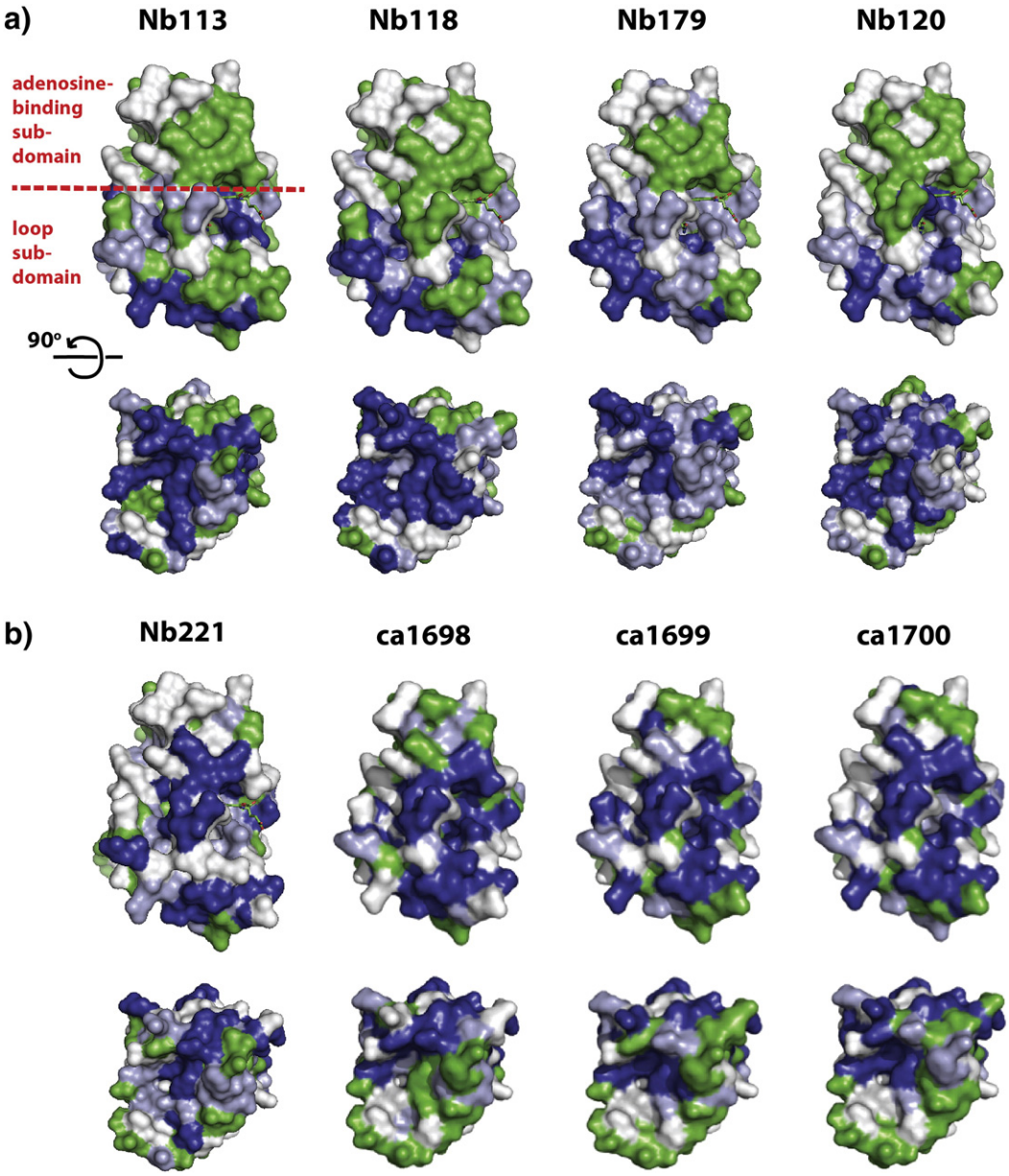

Fig. 3. A selection of epitope maps determined by chemical shift perturbation NMR spectroscopy. (a) α-Epitope binders (b) β epitope binders. DHFR surface residues (PDB code 1RX2) are coloured as follows: i) strongly affected cross peaks (dark blue); ii) weakly affected cross peaks (light blue); un-perturbed cross peaks (green); iv) residues excluded from the analysis (white). Two maps that differ by a 90° rotation are shown for each nanobody. Folate bound at the active site is indicated in stick representation.

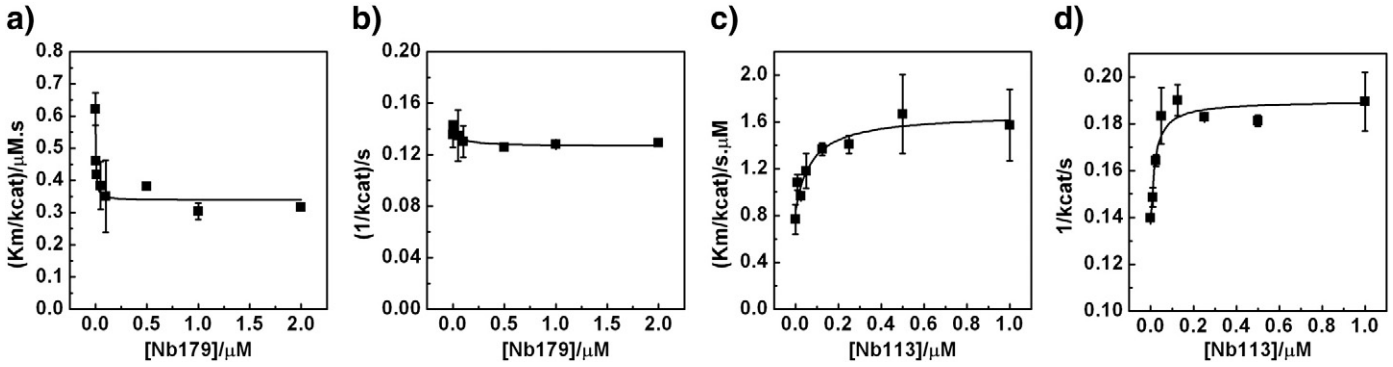

Fig. 4. Steady-state kinetic analysis of Nb179 (a and b) and Nb113 (c and d) at 10 μM H_2F (pH 7.0) at 25 °C. Nonlinear fits to Eq. (1) are shown. Error bars represent the standard deviation from two experiments performed on the same day.

NMR. A selection of nanobodies was chosen for analysis that displayed different kinetic properties (including partial inhibition and activation). Epitope residues were identified by comparing [^{15}N-DHFR:folate] ^{1}H–^{15}N HSQC spectra in the presence and absence of nanobody (SI Fig. 5). DHFR residues whose cross peaks undergo the largest chemical shifts upon addition of nanobody are assumed to be located at the epitope. In spite of the diverse kinetic effects shown by the selected nanobodies, the epitope maps fall into two distinct types. The first region (epitope α) consists of residues clustered on the loop subdomain comprising strands A, F, G and H and loops FG, and GH (Fig. 3a). This epitope is clearly distal to the NADPH and substrate binding sites and therefore represents an allosteric site. The second epitope region (epitope β) consists of residues that are much more widely dispersed in the region of the folate binding site (Fig. 3b). All of the nanobodies selected from the (−) library bind to epitope α while the nanobodies selected from the (+) library bind to epitope β (Table 1).

3.5. Detailed kinetic characterisation of epitope α binders confirms allosteric effector behaviour

The steady-state kinetic and NMR epitope mapping data indicate that nanobodies that bind to the same epitope region can display different allosteric effector properties. To investigate this phenomenon further, we examined the kinetic properties of the α epitope binders Nb179 and Nb113. Nb179 gives rise to hyperbolic activation kinetics with respect to NADPH, increasing $(k_{cat}/K_m)^{NADPH}$ 2-fold under saturating concentrations of nanobody (Fig. 4a and b). Nb113 gives rise to hyperbolic mixed inhibition kinetics (i.e. partial inhibition) with respect to NADPH, with $(k_{cat}/K_m)^{NADPH}$ and $(k_{cat})^{NADPH}$ decreasing 2-fold and 1.4-fold, respectively (Fig. 4c and d). Hyperbolic inhibition and activation kinetics are characteristic properties of allosteric effectors [8].

3.6. Crystallographic analysis of an allosteric inhibitor and allosteric activator bound at the α epitope

The allosteric effector mechanisms of the activator Nb179 and inhibitor Nb113 were examined in greater detail using X-ray crystallography (Figs. 5 and 6). Two crystal structures of DHFR in complex with Nb113 were solved: the [DHFR:Nb113] binary complex and the [DHFR:folate:Nb113] ternary complex. The two structures are very similar (r.m.s. differences in Cα positions for DHFR and Nb113 are 0.25 Å and 0.19 Å, respectively) and will be discussed together. For Nb179, we determined the [DHFR:folate:$NADP^+$:Nb179] ternary complex. Many of the structural features in the Nb113 and Nb179 complexes are shared. The epitopes are located >10 Å from the active site, coinciding with their predicted α epitopes identified by chemical shift perturbation NMR. The nanobodies interact principally with the N-terminal end of the Met20 loop and the FG loop of DHFR, using residues from CDR2 and CDR3. The bonding pattern in this region is largely conserved between the two nanobodies, despite sequence differences in CDR2 and CDR3

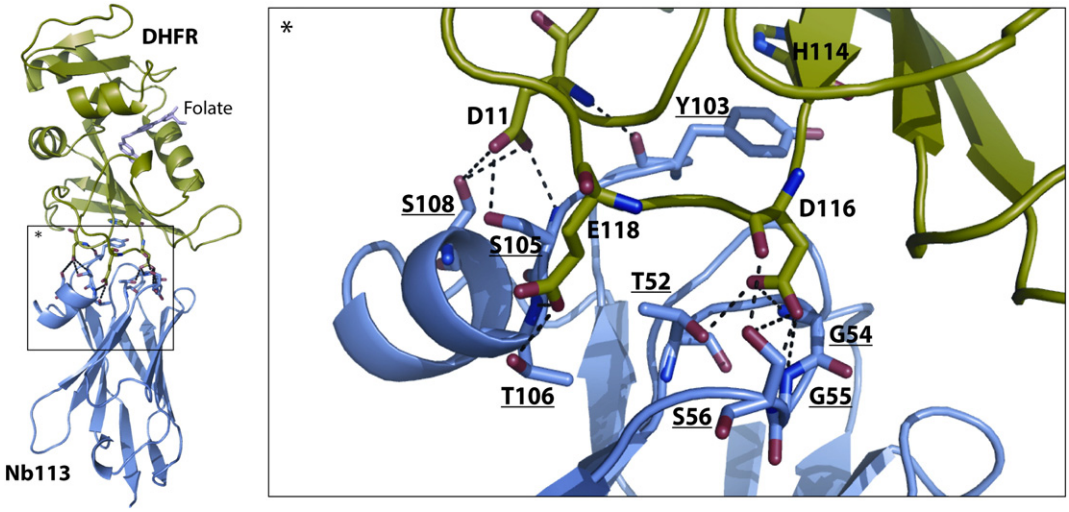

Fig. 5. Crystal structure of the [DHFR:folate:Nb113] complex. DHFR (green) and Nb113 (blue) are shown in cartoon representation, and folate is shown in stick representation. A zoom of the interface region is shown with residues participating in polar interactions (Nb113 residues are underlined).

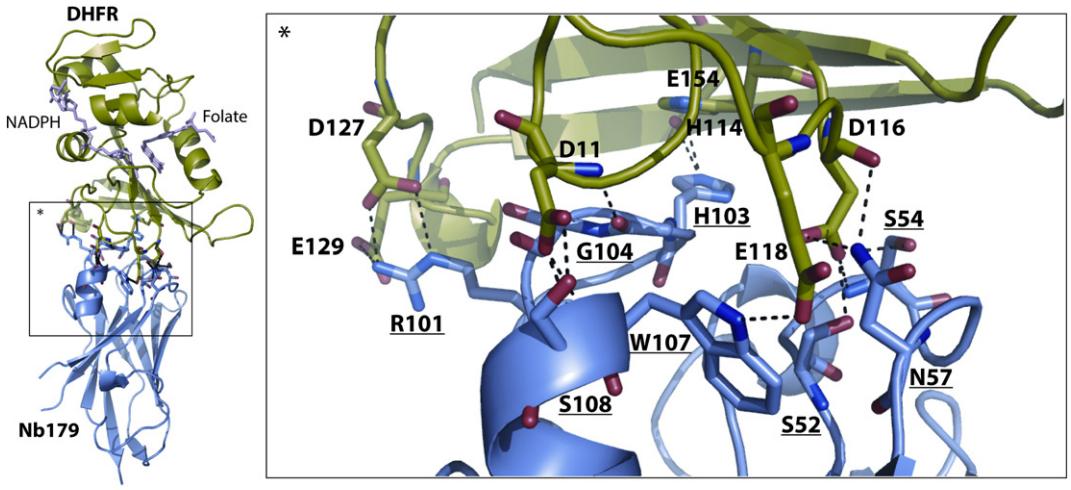

Fig. 6. Crystal structure of the [DHFR:folate:NADP$^+$:Nb179] complex. DHFR (green) and Nb113 (blue) are shown in cartoon representation; folate and NADP$^+$ are shown in stick representation. A zoom of the interface region is shown with residues participating in polar interactions (Nb179 residues are underlined).

(Tables 2 and 3). For example, Tyr103 of Nb113 and His 114 of Nb179 make π-stacking interactions with DHFR residue His114. One notable difference is the presence of salt bridges between the FG loop and Nb179 CDR3 that are absent in the Nb113 structures (Fig. 6).

3.7. No change in DHFR conformation at the α epitope is observed upon binding of Nb113 or Nb179

To determine whether Nb113 or Nb179 binding to DHFR causes structural change of DHFR, we examined r.m.s. differences of Cα positions between bound and un-bound DHFR. The [DHFR:folate:NADP$^+$:Nb179] structure has an open Met20 loop conformation and was therefore compared to the open [E:folate:NADP$^+$] crystal structure (PDB code 1RB2). No significant r.m.s. difference in Cα position is observed, indicating that the DHFR conformation does not change upon Nb179 binding (SI Fig. 6). The [E:Nb113] structure, which has an occluded Met20 loop conformation, was compared with the occluded [E:folate] crystal structure (PDB code 1RX7). Three regions of the DHFR sequence show r.m.s. differences >1 Å: the Met20 loop, the region between helix C and sheet C, and the FG loop (Fig. 7b). None of these regions take part in the nanobody:DHFR interface and therefore we conclude that no change in epitope structure occurs upon Nb113 binding (Fig. 7d). Furthermore, residues in the region between helix C and sheet C show unperturbed chemical shifts, suggesting that the r.m.s. differences observed in this region may arise from crystal packing effects (Fig. 7e). However, residues in the Met20 and FG loops do show perturbed chemical shifts. Therefore, it is possible that Nb113 induces conformational changes at regions distal to the epitope.

3.8. Nanobody binding to the β epitope leads to an unanticipated mode of inhibition

Previously, we showed that Nb216 binding to the β-epitope region can give rise to allosteric effects, namely hyperbolic mixed inhibition

Table 2
DHFR:Nb113 interactions in the E:FOL:Nb113 complex.

DHFR residue (chain A)	Secondary structure	Nb113 residue (chain D)	Framework or CDR loop	Type of interaction	Distance (Å)	Buried surface area (Å^2)
[a]V10	Met20	R104	CDR3	Hydrophobic		61
V10	Met20	S105	CDR3	Hydrophobic		
[a]D11 N	Met20	Y103 O	CDR3	H-bond	2.98	72
D11 OD1	Met20	S105N	CDR3	H-bond	3.04	
D11 OD1	Met20	S105 OG	CDR3	H-bond	3.59	
D11 OD1	Met20	S108 OG	CDR3	H-bond	3.09	
D11 OD2	Met20	S105 OG	CDR3	H-bond	2.56	
D11 OD2	Met20	S108 OG	CDR3	H-bond	3.00	
[a]H114	F strand	Y103	CDR3	π stacking		50
[a]I115	FG loop	W53	CDR2	Hydrophobic		3
I115 O	FG loop	W53 NE1	CDR2	H-bond	3.87	
[a]D116	FG loop	W53	CDR2	Hydrophobic		92
D116 O	FG loop	S56 OG	CDR2	H-bond	2.73	
D116 OD1	FG loop	T52 OG1	CDR2	H-bond	2.60	
D116 OD1	FG loop	G54N	CDR2	H-bond	3.01	
D116 OD2	FG loop	G55N	CDR2	H-bond	3.19	
D116 OD2	FG loop	S56N	CDR2	H-bond	2.88	
D116 OD2	FG loop	S56 OG	CDR2	H-bond	2.76	
[a]E118 OE2	FG loop	T106N	CDR3	H-bond	2.64	104
E118 OE2	FG loop	T106 OG1	CDR3	H-bond	2.57	
F140	G strand	W53	CDR2	Hydrophobic		70
[a]S150	H strand	W53	CDR2	Hydrophobic		17
S150 OG	H strand	G54 O	CDR2	H-bond	3.65	
Y151	H strand	W53	CDR2	Hydrophobic		2
C152	H strand	W53	CDR2	Hydrophobic		21
C152	H strand	Y103	CDR3	Hydrophobic		

[a] Conformational exchange observed on the millisecond timescale in DHFR reaction intermediates and intermediate analogues (Boehr et al.).

Table 3
DHFR:Nb179 interactions.

DHFR residue (chain A)	Secondary structure	Nb179 residue (chain D)	Framework or CDR loop	Type of interaction	Distance (Å)	Buried surface area (Å^2)
[a]V10	Met20 loop	W107	CDR3	Hydrophobic		40
[a]D11 N	Met20 loop	G104 O	CDR3	H-bond	2.48	78
D11 OD1	Met20 loop	S108N	CDR3	H-bond	3.01	
D11 OD1	Met20 loop	W107N	CDR3	H-bond	3.17	
D11 OD2	Met20 loop	S108 OG	CDR3	H-bond	2.49	
[a]H114	F strand	W53	CDR2	Hydrophobic		50
H114	F strand	H103	CDR3	π stacking		
[a]D116 O	FG loop	N57 ND2	CDR2	H-bond	3.06	110
D116 OD1	FG loop	N57 ND2	CDR2	H-bond	2.81	
D116 OD2	FG loop	S54N	CDR2	H-bond	3.12	
D116 OD2	FG loop	S54 OG	CDR2	H-bond	2.82	
D116 OD2	FG loop	S52 OG	CDR2	H-bond	2.55	
D116 OD2	FG loop	W53N	CDR2	H-bond	3.89	
[a]E118 OE2	FG loop	W107 NE1	CDR3	H-bond	2.98	66
E118 OE2	FG loop	K111 NZ	CDR3	Salt bridge	3.59	
D127 OD1	FG loop	R101 NH2	CDR3	Salt bridge	2.93	35
D127 OD1	FG loop	R101 NE	CDR3	Salt bridge	3.34	
D127 OD2	FG loop	R101 NE	CDR3	Salt bridge	3.42	
E129 OE2	FG loop	R101 NH2	CDR3	Salt bridge	3.25	19
P130	FG loop	P102	CDR3	Hydrophobic		59
C152	H strand	W53	CDR2	Hydrophobic		20
E154 OE1	H strand	H103 NE2	CDR3	Salt bridge	3.25	13

[a] Conformational exchange observed on the millisecond timescale in DHFR reaction intermediates and intermediate analogues (Boehr et al.).

kinetics [13]. In order to understand the structural basis of the kinetic effects observed with nanobodies that bind in the vicinity of the β-epitope (Table 1), we determined the crystal structure of ca1698 in complex with DHFR (Fig. 8a). ca1698 binds to DHFR in a sideways orientation, using residues from all three CDR regions and framework 2. This binding orientation results in a large (883.7 Å^2) binding surface area (BSA), and explains to a large extent the dispersed nature of the predicted ca1698 NMR epitope (Fig. 3b). Almost one third of the BSA in the [DHFR:ca1698] complex contains residues from the Met20 loop, and another third from helix C and the strand C–helix C loop (Table 4). Notably, the CDR3 of ca1698 extends into the substrate binding pocket (Fig. 8a). Thus, ca1698 is an active site binder. We anticipated that the occupancy of the substrate binding site by CDR3 would lead to competitive inhibition with respect to DHF. Surprisingly, a detailed kinetic

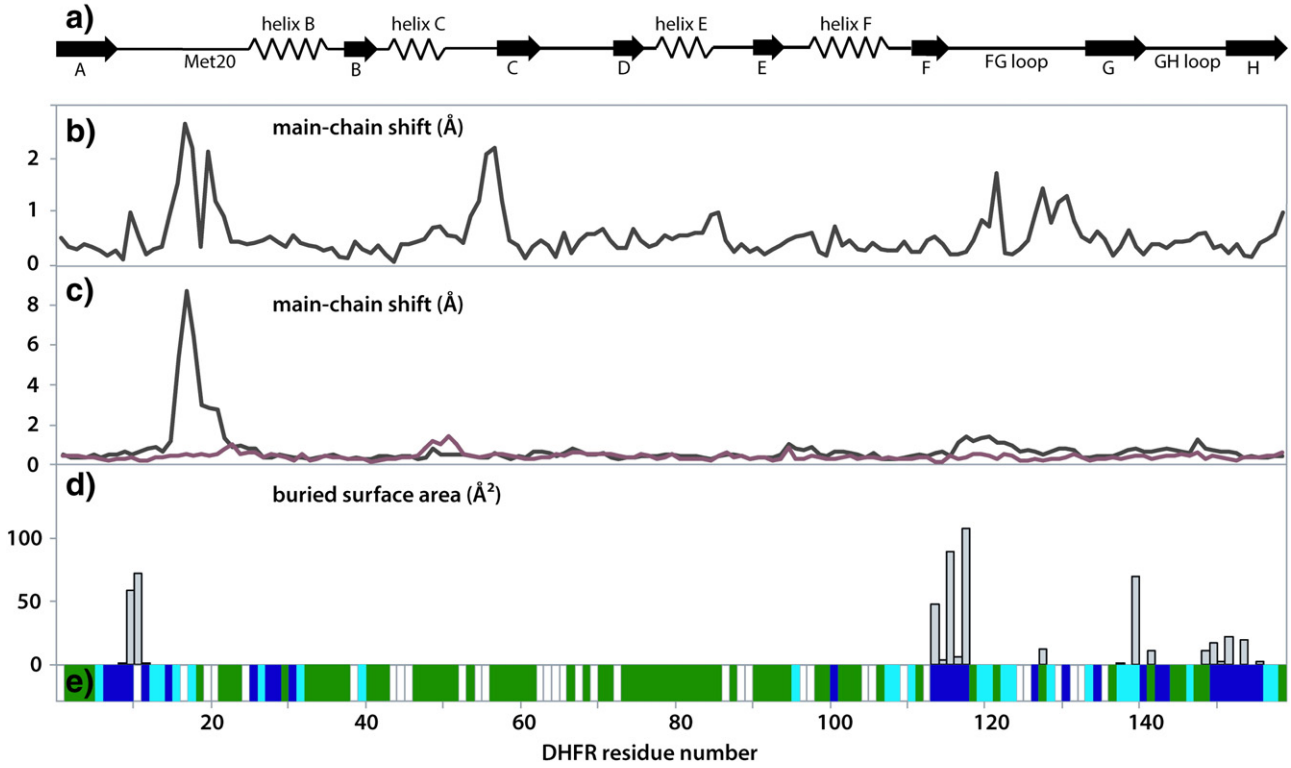

Fig. 7. Combined properties of the [DHFR:Nb113] and [DHFR:folate:Nb113] complexes. (a) Schematic representation of the DHFR secondary structural elements. (b) r.m.s. deviations of Cα positions between the [DHFR:Nb113] and [DHFR:folate] structure (PDB code 1RX7). This pair was chosen for comparison because of their similar crystallographic resolutions. (c) RMS differences in Cα positions between the occluded and closed forms of DHFR (1RX6–1RX1, black trace), and between two closed forms for comparison (1RX2–1R1, red trace). (d) Bar graph of the buried surface area (BSA) of the [DHFR:Nb113] complex calculated using PISA. (e) The predicted Nb113 NMR epitope.

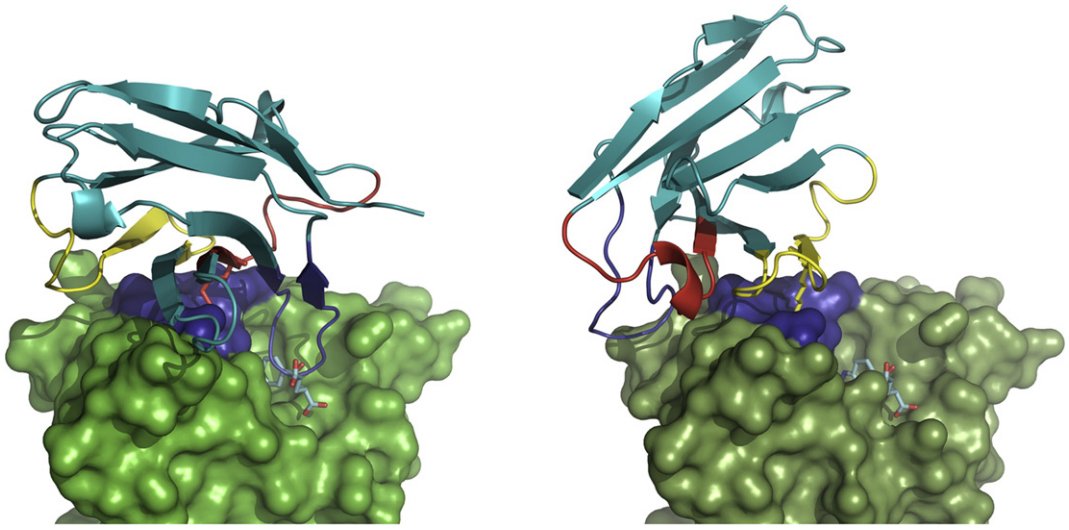

Fig. 8. Crystal structures of two β-epitope binders (left) [DHFR:ca1698] and (right) [DHFR:Nb216]. DHFR is shown in surface representation, with the Met20 loop region highlighted (dark blue). Folate is shown in stick representation for illustrative purposes. Nanobodies are shown in cartoon representation, with the CDR1, CDR2 and CDR3 regions coloured red, yellow and blue, respectively. The conserved lysine that interacts with the Met20 loop is shown in stick representation.

analysis showed that ca1698 gives rise to mixed linear inhibition kinetics with respect to DHF and not pure competitive inhibition (Fig. 9).

4. Discussion

We set out to isolate a diverse set of allosteric effector nanobodies that target DHFR to examine allosteric effects arising from protein–protein interactions. Two immunisations and three different phage panning strategies were used to increase nanobody diversity. While the panel of nanobodies displayed diverse sequences (SI Table 1) and diverse effector properties (Fig. 2), only two epitope regions were identified in the 18 nanobodies analysed by chemical shift perturbation NMR (Fig. 3 and SI Fig. 4). The nanobodies derived from the (−) library apparently bind to the α epitope while the nanobodies derived from the (+) library bind to the β epitope. This conclusion is supported by our failure to enrich (+) library phage during panning with methotrexate bead-bound DHFR, and the failure to obtain strong nanobody inhibitors during panning of the (−) library with the ELISA plate method (i.e. with unmasked DHFR). Interestingly, nanobody association rate constant (k_{on}) values are clustered according to the parent library (Fig. 1a). Nanobodies that bind to the α epitope display on average a 10-fold higher k_{on} than those that bind to the β epitope ($1.7 \pm 1.4\ \mu M^{-1}\ s^{-1}$ *versus* $0.16 \pm 0.08\ \mu M^{-1}\ s^{-1}$, respectively, Fig. 1b). The explanation for the clustering may therefore be structural in origin. For example, structural flexibility at the β epitope may reduce the equilibrium concentration of DHFR molecules that have an appropriate conformation to bind nanobody, resulting in lower apparent k_{on} values.

The reason why nanobodies from the (−) library target a different epitope than the (+) library nanobodies may be related to the absence or presence of Gerbu adjuvant during immunisation. Adjuvant effects have been observed with conventional antibodies [25]. Rabbits immunized with β-lactamase in the presence of Freund's adjuvant adjuvant generated a high proportion of antibodies that reacted with an exposed and flexible loop region of the native antigen (similar to the DHFR β epitope). By contrast, the antibodies produced by immunisation without

Table 4
DHFR:ca1698 interactions.

DHFR residue	Secondary structure	Ca1698 residue	Framework or CDR loop	Type of interaction	Distance (Å)	Buried surface area (Å^2)
E17 O	Met20 loop	K33 NZ	CDR1	Salt bridge	2.81	62
E17 OE2	Met20 loop	K33 NZ	CDR1	Salt bridge	2.89	
N18 ND2	Met20 loop	V31 O	CDR1	H-bond	2.82	116
N18 ND2	Met20 loop	R99 O	CDR3	H-bond	3.29	
N18 O	Met20 loop	T53N	CDR2	H-bond	2.85	
N18 O	Met20 loop	T53 OG1	CDR2	H-bond	3.09	
A19 0	Met20 loop	N54 OD1	CDR2	H-bond	3.24	54
M20 O	Met20 loop	K33 NZ	CDR1	H-bond	3.03	9
P21	Met20 loop	T52	CDR2	Hydrophobic	3.44	67
W22 O	Met20 loop	K33 NZ	CDR1	H-bond	2.82	21
W22	Met20 loop	L50	Framework 2	Hydrophobic	3.67	
N23 ND2	Met20 loop	Y37 OH	Framework 2	H-bond	2.79	71
L28	Helix B	L101	CDR3	Hydrophobic	3.63	40
F31	Helix B	L101	CDR3	Hydrophobic	3.87	38
E48 O	Helix C	R99 NH2	CDR3	H-bond	3.69	10
S49	Helix C	R99	CDR3	H-bond	2.25	17
I50	Helix C	A102	CDR3	Hydrophobic	3.72	53
R52 NE	Helix C/strand C loop	A102 O	CDR3	H-bond	2.77	73
R52 NH2	Helix C/strand C loop	A102 O	CDR3	H-bond	2.74	
L54	Helix C/strand C loop	A102	CDR3	Hydrophobic	3.67	21
A145 O	GH loop	L47N	Framework 2	H-bond	2.7	52
Q146 NE2	GH loop	R45 O	Framework 2	H-bond	3.06	67

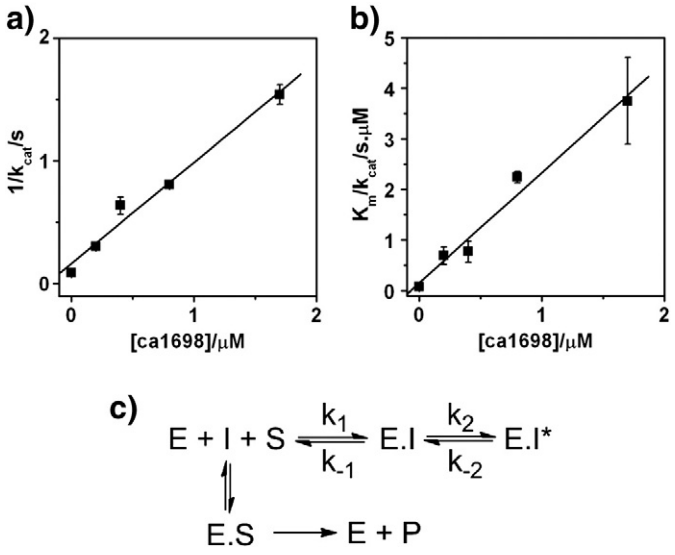

Fig. 9. Steady-state kinetic analysis of ca1698. (a and b) Plots of $(1/k_{cat})^{DHF}$ and $(K_m/k_{cat})^{DHF}$ *versus* [ca1698] at 50 μM NADPH, pH 7.0 and 25 °C. Linear fits of the $(K_m/k_{cat})^{DHF}$ and $(1/k_{cat})^{DHF}$ *versus* [ca1698] plots to Eqs. (2) and (3) (Methods) gives $k_{cat} = 6.1\ s^{-1}$, $k_{cat}/K_m = 6.6\ \mu M^{-1}\ s^{-1}$, $K_{ic} = 0.03 \pm 0.01\ \mu M$ and $K_{iu} = 0.20\ \mu M$. Error bars represent the standard deviation from two experiments. (c) Linear mixed-type inhibition scheme.

adjuvant recognised multiple (non-flexible) regions of the antigen (similar to the α epitope). Whether Gerbu adjuvant influences the nanobody (heavy chain antibody) response in llamas in the same way as conventional IgG antibodies in rabbits requires further study with a larger set of llamas for a statistical meaningful comparison.

Although the DHFR steady-state screening method used to screen nanobody effector properties does not permit identification of kinetic mechanism, it does allow an assessment of effector diversity and the identification of likely allosteric effector candidates (Fig. 2). It should be noted that more detailed kinetic analyses, as performed for Nb113 and Nb179 (Fig. 4), may yet reveal further allosteric effector antibody candidates. A key finding in the work here is that nanobodies that bind to the same epitope region can display contrasting allosteric effector properties. The X-ray crystal structures of DHFR bound to Nb113 and Nb179 at the α epitope provide some insight into this phenomenon (Figs. 5 and 6). Although Nb113 and Nb179 display contrasting effector properties (hyperbolic inhibition and activation kinetics, respectively), the pattern of bonding interactions at their epitopes is very similar. One difference that may be relevant is the presence of salt bridges between Nb179 CDR3 and the FG loop that are absent in the Nb113 structures.

The magnitude of the allosteric inhibition/activation observed with Nb113 and Nb179 is much smaller than that observed for the β-epitope binder Nb216 [13]. In the case of Nb216, the inhibition was shown to arise from the nanobody constraining the Met20 loop in an occluded conformation. This prevents the transient formation of the closed conformation that is necessary for the normal catalytic cycle to take place. More generally, enzyme catalysis is expected to be perturbed whenever an antibody binds to an epitope that undergoes conformational change during catalysis. For Nb113 and Nb179, the extent of conformation change that occurs at the α epitope during catalysis can be estimated by comparison of closed and occluded DHFR structures (specifically, the r.m.s; differences in Cα positions of DHFR during the catalytic cycle, Fig. 7c). The greatest r.m.s difference occurs in the Met20 loop; however, neither Nb113 nor Nb179 binds to this region (in contrast to Nb216 and ca1698). A smaller change in r.m.s. Cα position also occurs in the vicinity of 117–124 which does overlap with the Nb113 and Nb179 epitopes. It is therefore possible that binding of Nb113 and Nb179 to this region disrupts DHFR conformational change, leading to altered DHFR activity. While the (weak) stabilisation of the occluded state by Nb113 could explain its inhibitory properties, it is not obvious how conformational constraint of DHFR by Nb179 could result in an increased k_{cat}/K_m.

A second allosteric effector mechanism is the distortion of enzyme structure upon antibody binding. Effector antibodies that preferentially recognise a distorted epitope could arise if the clonal selection of B-lymphocytes was driven by a distorted form of the antigen. For Nb113 and Nb179, no distortion in their epitopes is apparent (Fig. 7 and SI Fig. 6). However, some distortion was apparent in the Nb113 crystal structures at two regions distal to the epitope (Fig. 7). This indicates a possible role for a third allosteric effector mechanism, namely altered protein dynamics. Distortion of DHFR structure distal to the epitope could result from a shift in the conformational ensemble of DHFR upon Nb113 binding. Large chemical shift perturbations at regions distal to the Nb113 and Nb179 epitopes were also seen in the NMR epitope maps (Fig. 3). It should be noted that the chemical shifts are influenced by multiple physical interactions and do not necessarily reflect a change in protein conformation. Many of the DHFR residues at the epitopes of Nb113 and Nb179 undergo conformational exchange on the millisecond timescale in the E:NADPH and E:NADP:THF forms of DHFR (Tables 2 and 3) [17]. Furthermore, both nanobodies bind to residues D11 and H114 which form part of an allosteric hotspot identified previously by statistical coupling analysis and allosteric domain insertion mapping [18]. Clearly, further experimental analysis (for example, NMR relaxation dispersion analysis) is required to determine how nanobody binding impacts DHFR dynamics.

To our knowledge, ca1698 is the first active-site directed antibody inhibitor described that gives rise to mixed-inhibition kinetics (Fig. 9). The observation of non-competitive inhibition by antibodies has generally been an indicator of allosteric inhibition [26]. Conversely, active-site directed antibodies are presumed to give rise to competitive inhibition kinetics [27]. However, it has been understood for many years that small molecule active-site directed inhibitors can behave as mixed or non-competitive inhibitors [28]. We discuss here two possible mechanisms for ca1698. Firstly, mixed-inhibition could arise from a two-step binding mechanism involving a slow isomerization step (Fig. 9c). In this mechanism, the initial binding of ca1698 to DHFR is followed by a slow isomerization step to form an EI* complex. The slow isomerisation step prevents rapid equilibration of the EI* form of inhibitor with the substrate-bound ES form in the steady-state, leading to mixed inhibition. Although no slow on-set inhibition was observed (data not shown), support for this model comes from SPR analysis of ca1698 binding to DHFR: the ca1698 SPR data better fit to a 2-step binding model than to a simple 1:1 binding model (SI Fig. 2).

Secondly, mixed inhibition could arise from the formation of an inactive [DHFR:NADPH:DHF:ca1698] dead-end complex under saturating concentrations of DHF, instead of an active [DHFR:NADPH:DHF] Michaelis complex. This co-binding of ca1698 and DHF would necessitate the exclusion of the CDR3 loop from the substrate binding pocket, a significant conformational change that would presumably lead to a significant loss in binding energy. Transient conformational change of the epitope in the nanobody-bound state was previously proposed to explain the observed partial inhibition displayed by Nb216 [13]. According to this mechanism, Nb216 inhibition is hyperbolic (instead of linear) because the [E:NADPH:DHF:Nb216] complex is catalytically active.

Comparison of the ca1698 crystal structure with the [DHFR:Nb216] crystal structure reveals two further interesting features (Fig. 8). Firstly, the binding orientations of Nb216 and ca1698 are related by a 180° rotation about an axis perpendicular to the DHFR surface. Secondly, both ca1698 and Nb216 bind to the Met20 loop of DHFR using a lysine residue (K33 and K59, respectively) whose side-chain inserts into a cavity adjacent to the Met20 loop (Fig. 10). This binding interaction could represent an instance of convergent evolution during affinity maturation. Firstly, this lysine residue is located in different CDRs in the two nanobodies (CDR1 of ca1698 and CDR2 of Nb216). Secondly, the

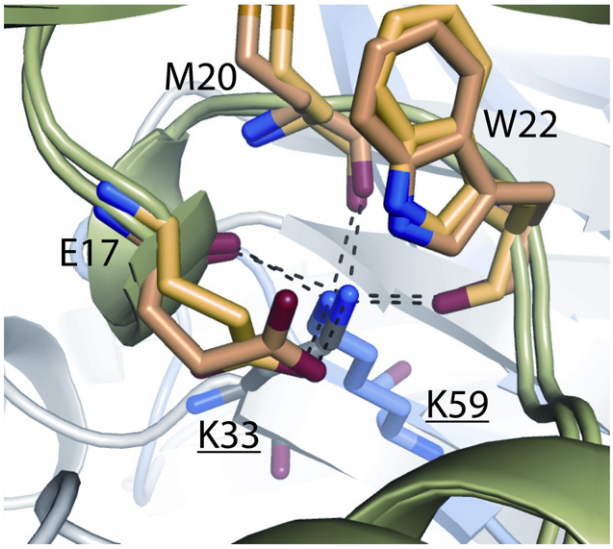

Fig. 10. Detail of the binding interaction between the Met20 loop region and the conserved lysine residues of ca1698 and Nb216.

framework 2 sequences of the two nanobodies clearly indicate that they originate from different germline B lymphocytes (only Nb216 contains the GLEW motif in the framework 2 region, indicating that a VH germline gene was used during somatic recombination).

In summary, we have shown that nanobodies that target only two epitope regions of DHFR can give rise to diverse kinetic effects. The small molecular size of the DHFR/nanobody system provides new opportunities to better understand structure/activity relationships of allosteric and active-site directed nanobody effectors. Future studies should permit the role of protein dynamics in nanobody allosteric effectors to be assessed. We also envisage that the conclusion drawn from this work will help to better understand the mechanisms of other antibody effectors, including those used for therapeutic applications.

5. Accession number

Atomic coordinates and structure factors have been deposited in the PDB under the following PDB codes: **4FHB** (DHFR:folate:NADP:Nb179); **4EIZ** (DHFR:Nb113), **4EJ1** (DHFR:folate:Nb113), and **4EIG** (DHFR:ca1698).

Acknowledgements

We thank Dr. Els Pardon for the preparation of the phage library and for expert advice for the phage selection, and Nele Buys and Katleen Willibal for assistance with the phage display. This work was funded by Research Foundation-Flanders and the Flanders Interuniversity Institute for Biotechnology.

Appendix A. Supplementary Data

Supplementary data to this article can be found online at http://dx.doi.org/10.1016/j.bbapap.2013.07.010.

References

[1] J. Otlewski, F. Jelen, M. Zakrzewska, A. Oleksy, The many faces of protease-protein inhibitor interaction, EMBO J. 24 (2005) 1303–1310.
[2] B. Svensson, K. Fukuda, P.K. Nielsen, B.C. Bønsager, Proteinaceous α-amylase inhibitors, Biochim. Biophys. Acta 1696 (2004) 145–156.
[3] G.I. Yakovlev, V.A. Mitkevich, A.A. Makarov, Ribonuclease inhibitors, Mol. Biol. 40 (2006) 867–874.
[4] S.W. Pettigrew, Oligomeric interactions provide alternatives to direct steric modes of control of sugar kinase/actin/hsp70 superfamily functions by heterotropic allosteric effectors: inhibition of *E. coli* glycerol kinase, Arch. Biochem. Biophys. 492 (2009) 29–39.
[5] B.B. Au-Yeung, S. Deindl, L.-Y. Hsu, E.H. Palacios, S.E. Levin, J. Kriyan, A. Weiss, The structure, regulation, and function of ZAP-70, Immunol. Rev. 228 (2009) 41–57.
[6] F. Celada, R. Strom, Antibody-induced conformation changes in proteins, Q. Rev. Biophys. 5 (1972) 395–425.
[7] L.M. Andersen, P.A. Andreasen, I. Svendsen, J. Keemink, H. Østergaard, E. Persson, Antibody-induced enhancement of factor VIIa activity through distinct allosteric pathways, J. Biol. Chem. 287 (2012) 8994–9001.
[8] J.N. Barlow, K. Conrath, J. Steyaert, Substrate-dependent modulation of enzyme activity by allosteric effector antibodies, Biochim. Biophys. Acta 1794 (2009) 1259–1268.
[9] E. Shapira, R. Arnon, The mechanism of inhibition of papain by its specific antibodies, Biochemistry 6 (1967) 3951–3956.
[10] A.J. McNally, K. Motter, F. Jordan, A library of monoclonal antibodies to *Escherichia coli* K-12 pyruvate dehydrogenase complex, J. Biol. Chem. 270 (1995) 19736–19743.
[11] A. Beck, T. Wurch, C. Bailly, N. Corvaia, Strategies and challenges for the next generation of therapeutic antibodies, Nat. Rev. Immunol. 10 (2010) 345–352.
[12] S.G.F. Rasmussen, H.-J. Choi, J.J. Fung, E. Pardon, P. Casarosa, P.S. Chae, B.T. DeVree, D.M. Rosenbaum, F.S. Thian, T.S. Kobilka, A. Schnapp, I. Konetzski, R.K. Sunahara, S.H. Gellman, A. Pautsch, J. Steyaert, W.I. Weis, B.K. Kobilka, Structure of a nanobody-stabilized active state of the β2 adrenoceptor, Nature 469 (2011) 175–181.
[13] D. Oyen, V. Srinivasan, J. Steyaert, J.N. Barlow, Constraining enzyme conformational change by an antibody leads to hyperbolic inhibition, J. Mol. Biol. 407 (2011) 138–148.
[14] J.R. Schell, H.J. Dyson, P.E. Wright, Structure, dynamics and catalytic function of dihydrofolate reductase, Annu. Rev. Biophys. Biomol. Struct. 33 (2004) 119–140.
[15] V.C. Nashine, S. Hammes-Schiffer, S.J. Benkovic, Coupled motions in enzyme catalysis, Curr. Opin. Chem. Biol. 14 (2010) 644–651.
[16] M.R. Sawaya, J. Kraut, Loop and subdomain movements in the mechanism of *Escherichia coli* dihydrofolate reductase: crystallographic evidence, Biochemistry 36 (1997) 586–603.
[17] D.D. Boehr, D. McElheny, H.J. Dyson, P.E. Wright, The dynamic energy landscape of dihydrofolate reductase, Science 313 (2006) 1638–1642.
[18] D.C. Williams, D.C. Benjamin, R.J. Poljak, G.S. Rule, Global changes in amide hydrogen exchange rates for a protein antigen in complex with three different antibodies, J. Mol. Biol. 257 (1996) 866–876.
[19] R.L. Blakley, Crystalline dihydropterylglutamic acid, Nature 188 (1960) 231–232.
[20] K. Domanska, S. Vanderhaegen, V. Srinivasan, E. Pardon, F. Dupeux, J.A. Marquez, S. Giorgetti, M. Stoppini, L. Wyns, V. Bellotti, J. Steyaert, Atomic structure of a nanobody-trapped domain-swapped dimer of an amyloidogenic β2-microglobulin variant, Proc. Natl. Acad. Sci. U. S. A. 108 (2010) 1314–1319.
[21] A.Q. Abbady, A. Al-Mariri, M. Zarkawi, A. Al-Assad, S. Muyldermans, Evaluation of a nanobody phage display library constructed from a *Brucella*-immunised camel, Vet. Immunol. Immunopathol. 142 (2011) 49–56.
[22] C.J. Falzone, J. Cavanagh, M. Cowart, A.G. Palmer, C.R. Matthews, S.J. Benkovic, P.E. Wright, 1H, 15N and 13C resonance assignments, secondary structure, and the conformation of substrate in the binary folate complex of Escherichia coli dihydrofolate reductase, J. Biomol. NMR 4 (1994) 349–366.
[23] X. Huang, X. Yang, B.J. Luft, S. Koide, NMR identification of epitopes of Lyme disease antigen OspA to monoclonal antibodies, J. Mol. Biol. 281 (1998) 61–67.
[24] D. Paus, G. Winter, Mapping epitopes and antigenicity by site-directed masking, Proc. Natl. Acad. Sci. U. S. A. 103 (2006) 9172–9177.
[25] R. Ganesan, Y. Zhang, K.E. Landgraf, S.J. Lin, P. Moran, D. Kirchhofer, An allosteric anti-hepsin antibody derived from a constrained phage display library, Prot. Eng. Des. Sel. 25 (2012) 127–133.
[26] K. Decanniere, A. Desmyter, M. Lauwereys, M.A. Ghadroudi, S. Muyldermans, L. Wyns, A single-domain antibody fragment in complex with RNase A: non-canonical loop structures and nanomolar affinity using two CDR loops, Structure 7 (1999) 361–370.
[27] Y. Blat, Non-competitive inhibition by active site binders, Chem. Biol. Drug Des. 75 (2010) 535–540.
[28] K.A. Reynolds, R.N. McLaughlin, R. Ranaganathan, Hot spots for allosteric regulation on protein surfaces, Cell 147 (2011) 1564–1575.